PROCEEDINGS OF SCIENCE

AugerPrime Surface Detector Electronics: requirements, verification and performance

Martina Boháčová[a,*] **for the Pierre Auger Collaboration**[b]

[a] *Institute of Physics, Prague, Czech Republic*

[b] *Observatorio Pierre Auger, Av. San Martín Norte 304, 5613 Malargüe, Argentina*

Full author list: https://www.auger.org/archive/authors_icrc_2025.html

E-mail: spokespersons@auger.org

The Pierre Auger Observatory has recently undergone a major upgrade, called AugerPrime, tailored to answer the current most pressing questions in the ultra-high-energy cosmic ray (UHECR) detection. The AugerPrime upgrade consists of the addition, on top of each station, of a scintillator detector, to separate the muonic and electromagnetic component of the shower for better primary identification, and of a radio detector to measure the emission of air showers in 30-80 MHz range. An additional small diameter photomultiplier is installed in each station to increase the dynamic range for signal detection. New electronic modules, installed on all stations, provide a sufficient number of channels for the readout of the additional detectors, as well as faster sampling, increased dynamic range and processing capability. In this contribution we summarize the performance of the new electronic modules with respect to the requirements, describe the verification procedure and give the results in the laboratory tests compared to the performance in the field.

39th International Cosmic Ray Conference (ICRC2025)
15 – 24 July, 2025
Geneva, Switzerland

ICRC 2025
The Astroparticle Physics Conference
Geneva July 15-24, 2025

*Speaker

PoS(ICRC2025)197

1. The Piere Auger Observatory and the AugerPrime upgrade

The Pierre Auger Observatory features a large detection area collecting unprecedented event statistics, and a combination of several detection techniques that allows one to lower the systematic uncertainties of the measurements. The Surface detector (SD) array is formed by 1600 water-Cherenkov detectors (WCD) placed in a triangular grid with 1500 m spacing (SD-1500) on the area of around 3000 km^2. The SD-1500 array is fully efficient above 3×10^{18} eV and continuously samples the extensive air showers (EAS) generated by the interaction of primary UHECRs with atmospheric nuclei, with a duty cycle of nearly 100 %. A nested region within the SD-1500 array contains additional 61 WCDs in half distances (SD-750) and even at 433 m distances (SD-433), covering an area of about 27 km^2 and 2 km^2 respectively. This allows us to lower the energy threshold of the Observatory below 10^{17} eV. The WCDs are overseen by 27 fluorescence telescopes located along the boundary of the array, which observe the longitudinal profile of the air showers. The operation of the fluorescence detector (FD) is limited to clear moonless nights. A thorough description of the Observatory is given in [1].

After nearly 20 years of operation, the Observatory has been upgraded. The main scientific aspects motivating the upgrade are the following: understand the origin of flux suppression, identify the sources of UHECRs, solve the discrepancy between hadronic interaction models and the measured shower parameters, and look for possible effects beyond the standard model. The upgrade aims at resolving these issues by obtaining more information on the mass composition of cosmic rays at the highest energies. Each WCD has been equipped with a 4 m^2 plastic scintillator mounted on the top (Surface Scintillator Detector or SSD). The two detectors will provide complementary information about the electromagnetic and muonic components of the shower. An additional Radio Detector (RD) is mounted on top of each WCD to observe the radio signals in the 30 – 80 MHz band from inclined showers to add yet another measurement of the electromagnetic component. A small PMT (SPMT), which is accompanying the three large PMTs from the baseline design inside the WCD, further extends the dynamic range and allows one to study signals closer to the shower core. Finally, underground muon detectors (UMD) are deployed near 61 stations of the denser area (SD-750 and SD-433) to provide a direct measurement of the muonic component of the EAS. A more powerful, modernized electronics was installed in each WCD interfacing the additional detectors together with the original ones. A detailed description of the SD electronics upgrade can be found in [2] and is summarized below. A comprehensive description of the Observatory upgrade can be found in [3].

The deployment of the pre-production and production electronics, together with SPMTs and SSDs, started in mid-2020 and was completed in July 2023. Commissioning studies are in progress since December 2020, to monitor various performance parameters. The installation of the RD detectors started in mid-2023 and was completed by the end 2024. The installation of UMD is well advanced and is expected to be completed in 2025.

2. Requirements and design of the Surface Detector electronics upgrade

The general requirement for the electronics upgrade was to increase the data quality exploiting faster sampling for Analog-Digital-Converter (ADC) traces, better timing accuracy, increased

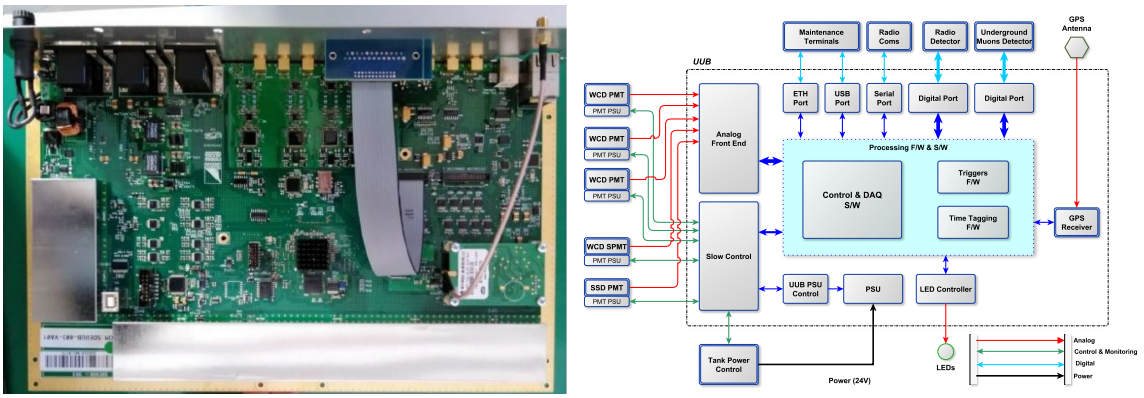

Figure 1: *Left:* UUB including front panel, GPS receiver and shielding covers. *Right:* Electrical interfaces of the UUB.

dynamic range, enhanced local trigger and processing capabilities, more powerful local station processor with a Field Programming Gate Array (FPGA), and improved calibration and monitoring capabilities. Backwards-compatibility was assured by retaining the time span of the PMT traces and providing for digital filtering and down-sampling of the traces to emulate the previous triggers in addition to new ones, implemented in the FPGA firmware. The most important functional and configurational design features are: digitization of the anode signals from the PMTs at a sampling frequency of 120 MS/s with a resolution of 12 bit and 10 ADC analog input channels (for the three large PMTs and the SSD PMT with two gains each plus the SPMT and a spare channel). Event time tagging with a resolution of 5 ns and a stability better than 5% depending on temperature variations is achieved by implementing Synergy SSR-6TF timing GPS receivers. All the functions (except GPS receivers) are integrated on a single Upgraded Unified Board (UUB) including also power-supply unit with safety features. The total power consumption has to be kept on a minimum level and it currently amounts to about 14 W including all the interfaces. UUB is designed to fit into the preexisting RF-enclosure and cable connections are compatible with the previous electronics board (UB). The UUB architecture is designed with a Xilinx Zynq FPGA containing two embedded ARM Cortex A9 333 MHz microprocessors. The FPGA is connected to a 4 Gbit LP-DDR2 memory and a 1 Gbit Flash memory. The FPGA implements all basic digital functions such as the read-out of the ADCs, the generation of triggers, and the integration of GPS receiver, clock tree and memories. Two digital ports on the UUB enable communication with additional detector systems. The requirement of total RMS integrated noise at the ADC output below 0.5 LSB (Least Significant Bit) for the LG channel and 2 LSB for the HG channel is achieved by a careful analog design and the use of low noise dual ADC (AD9628). A powerful 16-bit RISC CPU ultra-low-power micro-controller (MSP430) is used for the PMT high-voltage control, the supervision of various supply voltages and monitoring of environmental sensors.

2.1 Production, testing, verification and deployment

The UUBs were manufactured by the A4F company (Angel4Future, Bari, Italy). Quality control and testing of the boards was performed at a test benches provided by the Auger Collaboration. As a first step of the testing procedure, the UUBs were subjected to an automatic optical inspection to

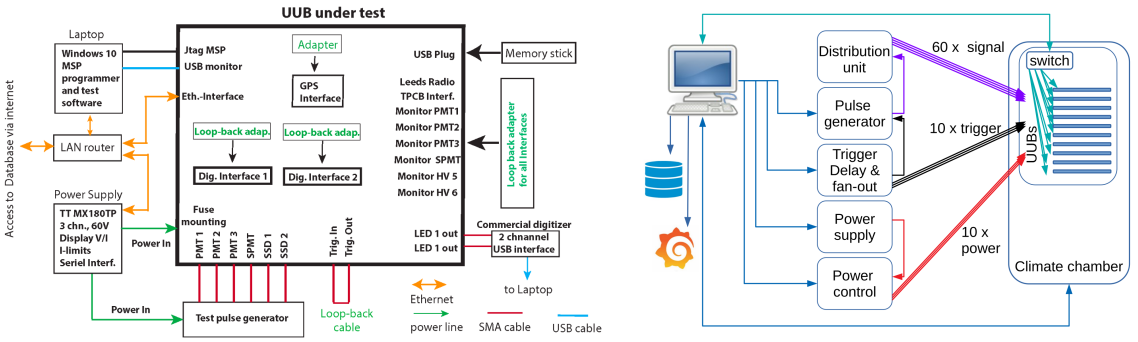

Figure 2: *Left:* Manufacturing test bench scheme. *Right:* ESS test bench scheme.

detect any missing components or soldering problems. The subsequent manufacturing test verifies all electrical lines and the basic functionality of the UUB. During the manufacturing test, an updated firmware for the MSP microcontroller and FPGA was installed . The scheme of the manufacturing test bench is shown in the left panel of Fig. 2.

The UUBs were then submitted to an Environmental Stress Screening (ESS), to characterize the behavior of the new electronics under changing environmental conditions typically observed at the Observatory site (see Fig. 5 the right panel for the typical temperature profile inside the electronics enclosure of WCD) and to provoke early failures. During the automated procedure a set of ten UUBs at a time were first subjected to burn-in (rapid temperature changes for 24 hours) with noise, baselines and temperature regularly monitored. In a second step, 10 temperature cycles, from -20°C to +70°C (temperature change of 3°C/min) were applied. The performance of each UUB was monitored at five different temperatures, in particular studying the noise, baseline and linearity dependence on temperature, the stability of the ADCs and the anti-alias filter, and a verifying of the over/under voltage protection. The scheme of the ESS test bench is shown in the right panel of Fig. 2, and a detailed description of the test procedure can be found in [4].

Several failures were encountered during the test procedure, such as ADC flipping bits, ADCs or baseline instabilities, or failures of the 3.3V converter, mainly due to nonconforming components and production faults. Most of these failures were mitigated by repairing and component exchange, yielding a final failure rate at production of about 1.3%.

After ESS, the UUBs were transported to the Pierre Auger Observatory, where they underwent a final verification and a full functionality test before deployment in the field. First, a visual inspection was performed to search for transportation damages. The UUBs were then assembled adding the GPS receiver, cables, connectors, front panel, and the complete setup was placed inside a protective RF-enclosure. The final end-to-end verification was performed before the whole assembly was taken to the field and integrated into each surface detector station.

3. Calibration

3.1 WCD and SSD calibration

Both detectors are continuously calibrated with background atmospheric muons. The charge histograms produced each minute show characteristic humps corresponding to the Vertical Equiv-

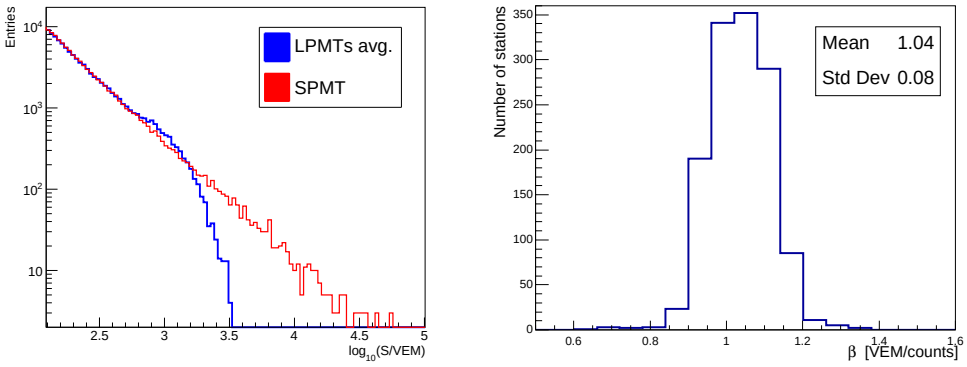

Figure 3: *Left:* Extension of the WCD dynamic range to 20 000 VEM using the small PMT. *Right:* Distribution of the average cross-calibration factors β on a single day, after the installation and setting of all the SPMTs in the array.

alent Muon (VEM) in the WCD and the Minimum Ionizing Particle (MIP) in the SSD. The mean measured charge values are about 1400 and 110 ADC channels, respectively for the VEM and MIP. In addition, 40% of the muons are measured by WCD and SSD in coincidence (corresponding to the overlapping area), which helps to significantly reduce the background and makes the VEM and MIP humps clearly distinguishable. Since this calibration is done every minute of the data taking, any long term temperature dependence of various components is taken into account during analysis of the shower data.

3.2 Cross-calibration of the SPMT

Limited by their photocathode dimension, the new small PMTs cannot be calibrated exploiting the same method as for the large PMTs, as only about one photoelectron per muon is recorded by the SPMT with respect to about 90 collected in the LPMT. For this reason, a new method was developed based on the minimization of the differences between the calibrated signal spectrum of the large WCD PMTs and that of the small PMT. The so-called β factor derived in this way is then used to cross-calibrate the SPMT, converting the collected charge measured in ADC channels into a signal in VEM. A dedicated selection of signals from local low energy showers is exploited, measured separately in each station at a rate of about 200 events/hour. The minimization is performed in a superposition region, where the signal is large enough for the SPMT, but not saturated in LPMTs. The logarithm of the charge spectrum in one upgraded WCD station is shown in the left panel of Fig. 3. Thanks to the SPMT, the dynamic range is extended to more than 20 000 VEM. In order to follow the daily evolution of the SPMT gain due to the temperature variations, the cross-calibration is performed in 8-hour sliding windows. In this way, a precision in the determination of the cross-calibration factor β of $\sim$2.2% is obtained. The stability of the β factor across the whole array is shown in the right panel of Fig. 3. A yearly evolution ot about $\pm$5% is expected, due to the seasonal variation of the average temperature in the field. Further details on the SPMT implementation and performance can be found in [5].

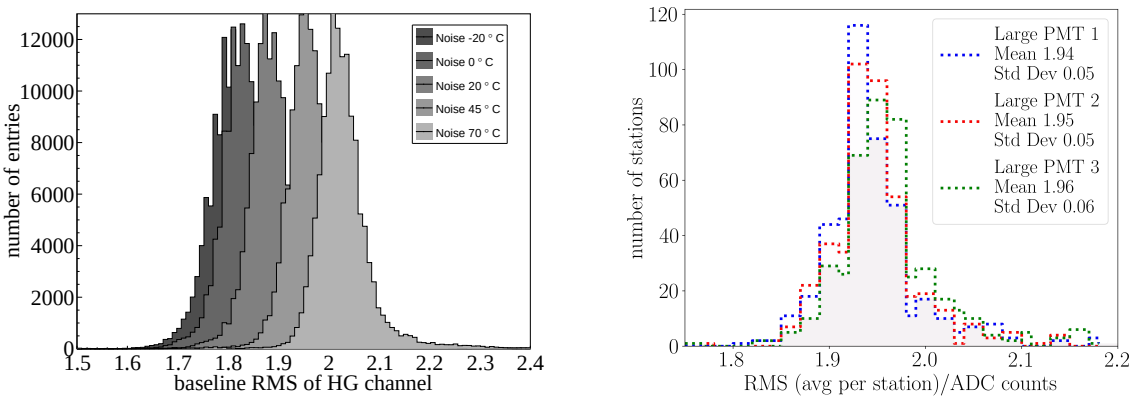

Figure 4: *Left:* Noise measured on the UUB high gain channels at the ESS test bench. All three Large PMTs for all UUBs are plotted together. *Right:* Noise of the HG channels of the individual PMTs as measured in the field.

4. Performance

4.1 Noise levels

The noise performance of each channel was verified in the ESS test bench. For the high-gain channel the noise was measured to slightly increase with temperature and to be below 2 ADC bins for most channels (as seen in the left panel of Fig. 4), meeting the requirements. The SSD high-gain channels show even better noise performance for all temperatures. The noise of the SPMT and the low-gain channels of LPMTs and SSD PMTs were measured to be around 0.5 ADC channel, again in agreement with the requirements. During field operation, the electronic modules are exposed to external environmental factors, affecting the connections to PMTs, the power system, and communication and timing systems, which can induce noise. Also the grounding quality, depending on field conditions, can impact the noise performance of the electronics. Compared to the previous UB electronics, the UUB has a factor 4 lower thresholds and is more susceptible to external noise. Sudden bursts of noise were observed in the traces on daily bases close to sunrise and were found to be connected with the battery charging. Modification of the tank power control board mitigated this problem. Enhanced battery maintenance, together with better cabling organization and better grounding, further improved noise levels in the field. Large spikes in trigger rates were observed in coincidence with distant lightning, which resulted in a data acquisition crash. This effect was tracked down to bi-polar signals observed in some traces. The problem was eliminated by a trigger conditioning algorithm applied in the FPGA before triggering, which removes bi-polar oscillations in the baseline while preserving the unipolar physics signal.

4.2 Time resolution

The upgraded electronics uses SSR-6TF timing GPS receivers to synchronize the detectors. These receivers are functionally compatible with the previous electronics and their intrinsic accuracy given by the manufacturer is 2 ns. The timing performance of the SSR-6FF GPS receiver was verified in the laboratory, relative to an FS275 GPS-disciplined rubidium atomic clock. The absolute timing accuracy was found to range from 2.3 ns (over timescales of a few seconds) up to about 6 ns (over

timescales of several hours). The relative timing accuracy between two receivers was measured in a climate chamber across a temperature range relevant for the electronics enclosure in the field, and reached 2.1 ns. The verification of the timing performance of the GPS SSR-6TF receivers mounted on UUBs after deployment in the field was done using a synchronization cable to send timing signals between two closely positioned ($\sim$ 20 m) WCDs, yielding a timing accuracy of about 5 ns, consistent with the lab measurements and the timing granularity as implemented on the UUB. Similar measurement performed using real showers reached an accuracy of 13 ns, which is, however, dominated by shower-to-shower fluctuations.

4.3 Trigger performance

A detailed description of the trigger implementation can be found in [2]. The Observatory is currently running with compatibility triggers, that is the traces are digitally filtered using a FIR Nyquist filter with a 20 MHz cut-off, and down sampled to 40 MHz (the rate of the UB electronics), by taking every third bin, and then the trigger algorithm of the former electronics is applied. This allows us to combine data sets from the previous phase of operation and from AugerPrime during the deployment period, without disturbance to the data taking. The new triggers, which take advantage of the full bandwidth, i. e. 120 MHz sampling rate of the traces are currently under development. In particular, a trigger for the Radio Detector has been developed and is currently being tested in a dedicated area of the array. The trigger performances of the previous and new electronics are compatible: the second-level trigger rates are about 20 Hz and the shower trigger rates are around 1 Hz for both types of electronics. The increased number of bins per trace and the additional channels result in an increased transfer time from 2 minutes to about 5 minutes per event. However, the available bandwidth is sufficient.

4.4 Dynamic range

The SD signal varies from few photoelectrons for stations far from the shower core to hundreds of thousands near the shower core. To achieve this large dynamic range the LPMT signal is passing through two amplification chains implemented within the electronics, as high gain (HG) and low gain (LG) channels. The highest particle densities are measured by the SPMT, with an anode-channel input at a single unitary gain. A detailed account of the SPMT implementation can be found in [2].

The average HG/LG ratio of the LPMT is given by the electronics design and was measured in the laboratory to be 31.7 $\pm$0.3 with less than 1% temperature dependence, which is fully compatible with the value obtained from suitable showers in the field, i.e. 31.7 $\pm$0.4, and represents a significant improvement in precision over the UB case, where the PMT last dynode signal was amplified and related to anode signal yielding 5% uncertainty. The SSD anode signal is also split in two, one amplified by 32, second divided by 4 yielding a nominal ratio of 128, and covering the same dynamic range as the associated WCD. The corresponding HG/LG ratio derived from the laboratory measurements was 125.8 $\pm$1.5, The slight discrepancy is caused by combined finite accuracies of the components.

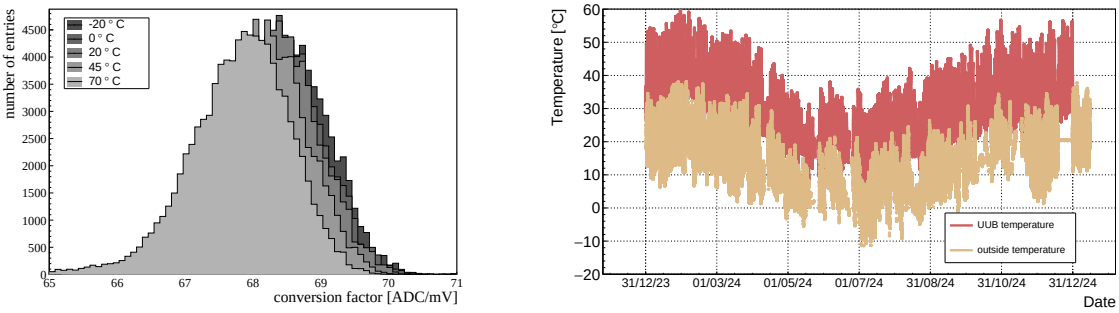

Figure 5: *Left:* Distribution of conversion factors from mV to ADC counts measured on the UUB high gain channels at the ESS test bench. Large PMT as well as SSD channels are included, no PMTs attached. The spread among the channels of all UUBs is larger than the temperature dependence. *Right:* Yearly temperature evolution inside the electronics enclosure of the SD station in relation to the outside temperature.

4.5 Temperature evolution

The stability of various parameters of the front-end electronics was studied in the temperature range relevant for the conditions in the Argentinian pampa. The temperature dependence of the gain of HG channels is plotted in Fig. 5. It can be noticed that the variation of the gain with temperature is smaller than the spread among individual UUBs and channels, when measured without PMTs. In the field, the seasonal variations of the detector response are dominated by the temperature dependence of the PMTs. It was demonstrated in the laboratory that the noise level is increasing with increasing temperature as expected. However, it stays within the requirements for most of the UUBs also at the highest tested temperature, not frequently reached in the field.

Conclusion

The Surface Detector electronics was upgraded to accommodate additional detectors and to enhance the experimental performances. The new features include a more powerful Xilinx Zynq-7020 FPGA for data prossing, faster ADCs sampling at 120MHz and up-to-date GPS receivers providing 5 ns timing resolution. The dynamic range of the Observatory is further increased by adding a SPMT inside the WCDs. Extensive tests of the electronics performed in the laboratory and in the field during the commissioning phase confirm that the design meets the requirements. The two years of the AugerPrime operation show good uniformity and stable long-term performance.

References

[1] A. Aab et al. [Pierre Auger Collaboration], NIM A 798, 2015, 172.

[2] A. Abdul Halim et al. [Pierre Auger Collaboration], JINST 18, 2023, P10016.

[3] A. Aab et al. [Pierre Auger Collaboration], AugerPrime - Preliminary Design Report, arXiv:1604.03637, 2016.

[4] M. Bohacova for the Pierre Auger Collaboration, PoS ICRC2019 (2021) 199

[5] G. Anastasi for the Pierre Auger Collaboration, PoS ICRC2023 (2024) 343

The Pierre Auger Collaboration

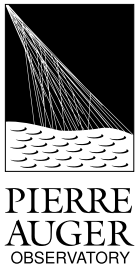

A. Abdul Halim[13], P. Abreu[70], M. Aglietta[53,51], I. Allekotte[1], K. Almeida Cheminant[78,77], A. Almela[7,12], R. Aloisio[44,45], J. Alvarez-Muñiz[76], A. Ambrosone[44], J. Ammerman Yebra[76], G.A. Anastasi[57,46], L. Anchordoqui[83], B. Andrada[7], L. Andrade Dourado[44,45], S. Andringa[70], L. Apollonio[58,48], C. Aramo[49], E. Arnone[62,51], J.C. Arteaga Velázquez[66], P. Assis[70], G. Avila[11], E. Avocone[56,45], A. Bakalova[31], F. Barbato[44,45], A. Bartz Mocellin[82], J.A. Bellido[13], C. Berat[35], M.E. Bertaina[62,51], M. Bianciotto[62,51], P.L. Biermann[a], V. Binet[5], K. Bismark[38,7], T. Bister[77,78], J. Biteau[36,i], J. Blazek[31], J. Blümer[40], M. Boháčová[31], D. Boncioli[56,45], C. Bonifazi[8], L. Bonneau Arbeletche[22], N. Borodai[68], J. Brack[f], P.G. Brichetto Orchera[7,40], F.L. Briechle[41], A. Bueno[75], S. Buitink[15], M. Buscemi[46,57], M. Büsken[38,7], A. Bwembya[77,78], K.S. Caballero-Mora[65], S. Cabana-Freire[76], L. Caccianiga[58,48], F. Campuzano[6], J. Caraça-Valente[82], R. Caruso[57,46], A. Castellina[53,51], F. Catalani[19], G. Cataldi[47], L. Cazon[76], M. Cerda[10], B. Čermáková[40], A. Cermenati[44,45], J.A. Chinellato[22], J. Chudoba[31], L. Chytka[32], R.W. Clay[13], A.C. Cobos Cerutti[6], R. Colalillo[59,49], R. Conceição[70], G. Consolati[48,54], M. Conte[55,47], F. Convenga[44,45], D. Correia dos Santos[27], P.J. Costa[70], C.E. Covault[81], M. Cristinziani[43], C.S. Cruz Sanchez[3], S. Dasso[4,2], K. Daumiller[40], B.R. Dawson[13], R.M. de Almeida[27], E.-T. de Boone[43], B. de Errico[27], J. de Jesús[7], S.J. de Jong[77,78], J.R.T. de Mello Neto[27], I. De Mitri[44,45], J. de Oliveira[18], D. de Oliveira Franco[42], F. de Palma[55,47], V. de Souza[20], E. De Vito[55,47], A. Del Popolo[57,46], O. Deligny[33], N. Denner[31], L. Deval[53,51], A. di Matteo[51], C. Dobrigkeit[22], J.C. D'Olivo[67], L.M. Domingues Mendes[16,70], Q. Dorosti[43], J.C. dos Anjos[16], R.C. dos Anjos[26], J. Ebr[31], F. Ellwanger[40], R. Engel[38,40], I. Epicoco[55,47], M. Erdmann[41], A. Etchegoyen[7,12], C. Evoli[44,45], H. Falcke[77,79,78], G. Farrar[85], A.C. Fauth[22], T. Fehler[43], F. Feldbusch[39], A. Fernandes[70], M. Fernandez[14], B. Fick[84], J.M. Figueira[7], P. Filip[38,7], A. Filipčič[74,73], T. Fitoussi[40], B. Flaggs[87], T. Fodran[77], A. Franco[47], M. Freitas[70], T. Fujii[86,h], A. Fuster[7,12], C. Galea[77], B. García[6], C. Gaudu[37], P.L. Ghia[33], U. Giaccari[47], F. Gobbi[10], F. Gollan[7], G. Golup[1], M. Gómez Berisso[1], P.F. Gómez Vitale[11], J.P. Gongora[11], J.M. González[1], N. González[7], D. Góra[68], A. Gorgi[53,51], M. Gottowik[40], F. Guarino[59,49], G.P. Guedes[23], L. Gülzow[40], S. Hahn[38], P. Hamal[31], M.R. Hampel[7], P. Hansen[3], V.M. Harvey[13], A. Haungs[40], T. Hebbeker[41], C. Hojvat[d], J.R. Hörandel[77,78], P. Horvath[32], M. Hrabovský[32], T. Huege[40,15], A. Insolia[57,46], P.G. Isar[72], M. Ismaiel[77,78], P. Janecek[31], V. Jilek[31], K.-H. Kampert[37], B. Keilhauer[40], A. Khakurdikar[77], V.V. Kizakke Covilakam[7,40], H.O. Klages[40], M. Kleifges[39], J. Köhler[40], F. Krieger[41], M. Kubatova[31], N. Kunka[39], B.L. Lago[17], N. Langner[41], N. Leal[7], M.A. Leigui de Oliveira[25], Y. Lema-Capeans[76], A. Letessier-Selvon[34], I. Lhenry-Yvon[33], L. Lopes[70], J.P. Lundquist[73], M. Mallamaci[60,46], D. Mandat[31], P. Mantsch[d], F.M. Mariani[58,48], A.G. Mariazzi[3], I.C. Mariş[14], G. Marsella[60,46], D. Martello[55,47], S. Martinelli[40,7], M.A. Martins[76], H.-J. Mathes[40], J. Matthews[g], G. Matthiae[61,50], E. Mayotte[82], S. Mayotte[82], P.O. Mazur[d], G. Medina-Tanco[67], J. Meinert[37], D. Melo[7], A. Menshikov[39], C. Merx[40], S. Michal[31], M.I. Micheletti[5], L. Miramonti[58,48], M. Mogarkar[68], S. Mollerach[1], F. Montanet[35], L. Morejon[37], K. Mulrey[77,78], R. Mussa[51], W.M. Namasaka[37], S. Negi[31], L. Nellen[67], K. Nguyen[84], G. Nicora[9], M. Niechciol[43], D. Nitz[84], D. Nosek[30], A. Novikov[87], V. Novotny[30], L. Nožka[32], A. Nucita[55,47], L.A. Núñez[29], J. Ochoa[7,40], C. Oliveira[20], L. Östman[31], M. Palatka[31], J. Pallotta[9], S. Panja[31], G. Parente[76], T. Paulsen[37], J. Pawlowsky[37], M. Pech[31], J. Pękala[68], R. Pelayo[64],

V. Pelgrims[14], L.A.S. Pereira[24], E.E. Pereira Martins[38,7], C. Pérez Bertolli[7,40], L. Perrone[55,47], S. Petrera[44,45], C. Petrucci[56], T. Pierog[40], M. Pimenta[70], M. Platino[7], B. Pont[77], M. Pourmohammad Shahvar[60,46], P. Privitera[86], C. Priyadarshi[68], M. Prouza[31], K. Pytel[69], S. Querchfeld[37], J. Rautenberg[37], D. Ravignani[7], J.V. Reginatto Akim[22], A. Reuzki[41], J. Ridky[31], F. Riehn[76,j], M. Risse[43], V. Rizi[56,45], E. Rodriguez[7,40], G. Rodriguez Fernandez[50], J. Rodriguez Rojo[11], S. Rossoni[42], M. Roth[40], E. Roulet[1], A.C. Rovero[4], A. Saftoiu[71], M. Saharan[77], F. Salamida[56,45], H. Salazar[63], G. Salina[50], P. Sampathkumar[40], N. San Martin[82], J.D. Sanabria Gomez[29], F. Sánchez[7], E.M. Santos[21], E. Santos[31], F. Sarazin[82], R. Sarmento[70], R. Sato[11], P. Savina[44,45], V. Scherini[55,47], H. Schieler[40], M. Schimassek[33], M. Schimp[37], D. Schmidt[40], O. Scholten[15,b], H. Schoorlemmer[77,78], P. Schovánek[31], F.G. Schröder[87,40], J. Schulte[41], T. Schulz[31], S.J. Sciutto[3], M. Scornavacche[7], A. Sedoski[7], A. Segreto[52,46], S. Sehgal[37], S.U. Shivashankara[73], G. Sigl[42], K. Simkova[15,14], F. Simon[39], R. Šmída[86], P. Sommers[e], R. Squartini[10], M. Stadelmaier[40,48,58], S. Stanič[73], J. Stasielak[68], P. Stassi[35], S. Strähnz[38], M. Straub[41], T. Suomijärvi[36], A.D. Supanitsky[7], Z. Svozilikova[31], K. Syrokvas[30], Z. Szadkowski[69], F. Tairli[13], M. Tambone[59,49], A. Tapia[28], C. Taricco[62,51], C. Timmermans[78,77], O. Tkachenko[31], P. Tobiska[31], C.J. Todero Peixoto[19], B. Tomé[70], A. Travaini[10], P. Travnicek[31], M. Tueros[3], M. Unger[40], R. Uzeiroska[37], L. Vaclavek[32], M. Vacula[32], I. Vaiman[44,45], J.F. Valdés Galicia[67], L. Valore[59,49], P. van Dillen[77,78], E. Varela[63], V. Vašíčková[37], A. Vásquez-Ramírez[29], D. Veberič[40], I.D. Vergara Quispe[3], S. Verpoest[87], V. Verzi[50], J. Vicha[31], J. Vink[80], S. Vorobiov[73], J.B. Vuta[31], C. Watanabe[27], A.A. Watson[c], A. Weindl[40], M. Weitz[37], L. Wiencke[82], H. Wilczyński[68], B. Wundheiler[7], B. Yue[37], A. Yushkov[31], E. Zas[76], D. Zavrtanik[73,74], M. Zavrtanik[74,73]

[1] Centro Atómico Bariloche and Instituto Balseiro (CNEA-UNCuyo-CONICET), San Carlos de Bariloche, Argentina

[2] Departamento de Física and Departamento de Ciencias de la Atmósfera y los Océanos, FCEyN, Universidad de Buenos Aires and CONICET, Buenos Aires, Argentina

[3] IFLP, Universidad Nacional de La Plata and CONICET, La Plata, Argentina

[4] Instituto de Astronomía y Física del Espacio (IAFE, CONICET-UBA), Buenos Aires, Argentina

[5] Instituto de Física de Rosario (IFIR) – CONICET/U.N.R. and Facultad de Ciencias Bioquímicas y Farmacéuticas U.N.R., Rosario, Argentina

[6] Instituto de Tecnologías en Detección y Astropartículas (CNEA, CONICET, UNSAM), and Universidad Tecnológica Nacional – Facultad Regional Mendoza (CONICET/CNEA), Mendoza, Argentina

[7] Instituto de Tecnologías en Detección y Astropartículas (CNEA, CONICET, UNSAM), Buenos Aires, Argentina

[8] International Center of Advanced Studies and Instituto de Ciencias Físicas, ECyT-UNSAM and CONICET, Campus Miguelete – San Martín, Buenos Aires, Argentina

[9] Laboratorio Atmósfera – Departamento de Investigaciones en Láseres y sus Aplicaciones – UNIDEF (CITEDEF-CONICET), Argentina

[10] Observatorio Pierre Auger, Malargüe, Argentina

[11] Observatorio Pierre Auger and Comisión Nacional de Energía Atómica, Malargüe, Argentina

[12] Universidad Tecnológica Nacional – Facultad Regional Buenos Aires, Buenos Aires, Argentina

[13] University of Adelaide, Adelaide, S.A., Australia

[14] Université Libre de Bruxelles (ULB), Brussels, Belgium
[15] Vrije Universiteit Brussels, Brussels, Belgium
[16] Centro Brasileiro de Pesquisas Fisicas, Rio de Janeiro, RJ, Brazil
[17] Centro Federal de Educação Tecnológica Celso Suckow da Fonseca, Petropolis, Brazil
[18] Instituto Federal de Educação, Ciência e Tecnologia do Rio de Janeiro (IFRJ), Brazil
[19] Universidade de São Paulo, Escola de Engenharia de Lorena, Lorena, SP, Brazil
[20] Universidade de São Paulo, Instituto de Física de São Carlos, São Carlos, SP, Brazil
[21] Universidade de São Paulo, Instituto de Física, São Paulo, SP, Brazil
[22] Universidade Estadual de Campinas (UNICAMP), IFGW, Campinas, SP, Brazil
[23] Universidade Estadual de Feira de Santana, Feira de Santana, Brazil
[24] Universidade Federal de Campina Grande, Centro de Ciencias e Tecnologia, Campina Grande, Brazil
[25] Universidade Federal do ABC, Santo André, SP, Brazil
[26] Universidade Federal do Paraná, Setor Palotina, Palotina, Brazil
[27] Universidade Federal do Rio de Janeiro, Instituto de Física, Rio de Janeiro, RJ, Brazil
[28] Universidad de Medellín, Medellín, Colombia
[29] Universidad Industrial de Santander, Bucaramanga, Colombia
[30] Charles University, Faculty of Mathematics and Physics, Institute of Particle and Nuclear Physics, Prague, Czech Republic
[31] Institute of Physics of the Czech Academy of Sciences, Prague, Czech Republic
[32] Palacky University, Olomouc, Czech Republic
[33] CNRS/IN2P3, IJCLab, Université Paris-Saclay, Orsay, France
[34] Laboratoire de Physique Nucléaire et de Hautes Energies (LPNHE), Sorbonne Université, Université de Paris, CNRS-IN2P3, Paris, France
[35] Univ. Grenoble Alpes, CNRS, Grenoble Institute of Engineering Univ. Grenoble Alpes, LPSC-IN2P3, 38000 Grenoble, France
[36] Université Paris-Saclay, CNRS/IN2P3, IJCLab, Orsay, France
[37] Bergische Universität Wuppertal, Department of Physics, Wuppertal, Germany
[38] Karlsruhe Institute of Technology (KIT), Institute for Experimental Particle Physics, Karlsruhe, Germany
[39] Karlsruhe Institute of Technology (KIT), Institut für Prozessdatenverarbeitung und Elektronik, Karlsruhe, Germany
[40] Karlsruhe Institute of Technology (KIT), Institute for Astroparticle Physics, Karlsruhe, Germany
[41] RWTH Aachen University, III. Physikalisches Institut A, Aachen, Germany
[42] Universität Hamburg, II. Institut für Theoretische Physik, Hamburg, Germany
[43] Universität Siegen, Department Physik – Experimentelle Teilchenphysik, Siegen, Germany
[44] Gran Sasso Science Institute, L'Aquila, Italy
[45] INFN Laboratori Nazionali del Gran Sasso, Assergi (L'Aquila), Italy
[46] INFN, Sezione di Catania, Catania, Italy
[47] INFN, Sezione di Lecce, Lecce, Italy
[48] INFN, Sezione di Milano, Milano, Italy
[49] INFN, Sezione di Napoli, Napoli, Italy
[50] INFN, Sezione di Roma "Tor Vergata", Roma, Italy

PoS(ICRC2025)197

[51] INFN, Sezione di Torino, Torino, Italy
[52] Istituto di Astrofisica Spaziale e Fisica Cosmica di Palermo (INAF), Palermo, Italy
[53] Osservatorio Astrofisico di Torino (INAF), Torino, Italy
[54] Politecnico di Milano, Dipartimento di Scienze e Tecnologie Aerospaziali , Milano, Italy
[55] Università del Salento, Dipartimento di Matematica e Fisica "E. De Giorgi", Lecce, Italy
[56] Università dell'Aquila, Dipartimento di Scienze Fisiche e Chimiche, L'Aquila, Italy
[57] Università di Catania, Dipartimento di Fisica e Astronomia "Ettore Majorana", Catania, Italy
[58] Università di Milano, Dipartimento di Fisica, Milano, Italy
[59] Università di Napoli "Federico II", Dipartimento di Fisica "Ettore Pancini", Napoli, Italy
[60] Università di Palermo, Dipartimento di Fisica e Chimica "E. Segrè", Palermo, Italy
[61] Università di Roma "Tor Vergata", Dipartimento di Fisica, Roma, Italy
[62] Università Torino, Dipartimento di Fisica, Torino, Italy
[63] Benemérita Universidad Autónoma de Puebla, Puebla, México
[64] Unidad Profesional Interdisciplinaria en Ingeniería y Tecnologías Avanzadas del Instituto Politécnico Nacional (UPIITA-IPN), México, D.F., México
[65] Universidad Autónoma de Chiapas, Tuxtla Gutiérrez, Chiapas, México
[66] Universidad Michoacana de San Nicolás de Hidalgo, Morelia, Michoacán, México
[67] Universidad Nacional Autónoma de México, México, D.F., México
[68] Institute of Nuclear Physics PAN, Krakow, Poland
[69] University of Łódź, Faculty of High-Energy Astrophysics,Łódź, Poland
[70] Laboratório de Instrumentação e Física Experimental de Partículas – LIP and Instituto Superior Técnico – IST, Universidade de Lisboa – UL, Lisboa, Portugal
[71] "Horia Hulubei" National Institute for Physics and Nuclear Engineering, Bucharest-Magurele, Romania
[72] Institute of Space Science, Bucharest-Magurele, Romania
[73] Center for Astrophysics and Cosmology (CAC), University of Nova Gorica, Nova Gorica, Slovenia
[74] Experimental Particle Physics Department, J. Stefan Institute, Ljubljana, Slovenia
[75] Universidad de Granada and C.A.F.P.E., Granada, Spain
[76] Instituto Galego de Física de Altas Enerxías (IGFAE), Universidade de Santiago de Compostela, Santiago de Compostela, Spain
[77] IMAPP, Radboud University Nijmegen, Nijmegen, The Netherlands
[78] Nationaal Instituut voor Kernfysica en Hoge Energie Fysica (NIKHEF), Science Park, Amsterdam, The Netherlands
[79] Stichting Astronomisch Onderzoek in Nederland (ASTRON), Dwingeloo, The Netherlands
[80] Universiteit van Amsterdam, Faculty of Science, Amsterdam, The Netherlands
[81] Case Western Reserve University, Cleveland, OH, USA
[82] Colorado School of Mines, Golden, CO, USA
[83] Department of Physics and Astronomy, Lehman College, City University of New York, Bronx, NY, USA
[84] Michigan Technological University, Houghton, MI, USA
[85] New York University, New York, NY, USA
[86] University of Chicago, Enrico Fermi Institute, Chicago, IL, USA

PoS(ICRC2025)197

[87] University of Delaware, Department of Physics and Astronomy, Bartol Research Institute, Newark, DE, USA

—

[a] Max-Planck-Institut für Radioastronomie, Bonn, Germany
[b] also at Kapteyn Institute, University of Groningen, Groningen, The Netherlands
[c] School of Physics and Astronomy, University of Leeds, Leeds, United Kingdom
[d] Fermi National Accelerator Laboratory, Fermilab, Batavia, IL, USA
[e] Pennsylvania State University, University Park, PA, USA
[f] Colorado State University, Fort Collins, CO, USA
[g] Louisiana State University, Baton Rouge, LA, USA
[h] now at Graduate School of Science, Osaka Metropolitan University, Osaka, Japan
[i] Institut universitaire de France (IUF), France
[j] now at Technische Universität Dortmund and Ruhr-Universität Bochum, Dortmund and Bochum, Germany

Acknowledgments

The successful installation, commissioning, and operation of the Pierre Auger Observatory would not have been possible without the strong commitment and effort from the technical and administrative staff in Malargüe. We are very grateful to the following agencies and organizations for financial support:

Argentina – Comisión Nacional de Energía Atómica; Agencia Nacional de Promoción Científica y Tecnológica (ANPCyT); Consejo Nacional de Investigaciones Científicas y Técnicas (CONICET); Gobierno de la Provincia de Mendoza; Municipalidad de Malargüe; NDM Holdings and Valle Las Leñas; in gratitude for their continuing cooperation over land access; Australia – the Australian Research Council; Belgium – Fonds de la Recherche Scientifique (FNRS); Research Foundation Flanders (FWO), Marie Curie Action of the European Union Grant No. 101107047; Brazil – Conselho Nacional de Desenvolvimento Científico e Tecnológico (CNPq); Financiadora de Estudos e Projetos (FINEP); Fundação de Amparo à Pesquisa do Estado de Rio de Janeiro (FAPERJ); São Paulo Research Foundation (FAPESP) Grants No. 2019/10151-2, No. 2010/07359-6 and No. 1999/05404-3; Ministério da Ciência, Tecnologia, Inovações e Comunicações (MCTIC); Czech Republic – GACR 24-13049S, CAS LQ100102401, MEYS LM2023032, CZ.02.1.01/0.0/0.0/16_013/0001402, CZ.02.1.01/0.0/0.0/18_046/0016010 and CZ.02.1.01/0.0/0.0/17_049/0008422 and CZ.02.01.01/00/22_008/0004632; France – Centre de Calcul IN2P3/CNRS; Centre National de la Recherche Scientifique (CNRS); Conseil Régional Ile-de-France; Département Physique Nucléaire et Corpusculaire (PNC-IN2P3/CNRS); Département Sciences de l'Univers (SDU-INSU/CNRS); Institut Lagrange de Paris (ILP) Grant No. LABEX ANR-10-LABX-63 within the Investissements d'Avenir Programme Grant No. ANR-11-IDEX-0004-02; Germany – Bundesministerium für Bildung und Forschung (BMBF); Deutsche Forschungsgemeinschaft (DFG); Finanzministerium Baden-Württemberg; Helmholtz Alliance for Astroparticle Physics (HAP); Helmholtz-Gemeinschaft Deutscher Forschungszentren (HGF); Ministerium für Kultur und Wissenschaft des Landes Nordrhein-Westfalen; Ministerium für Wissenschaft, Forschung und Kunst des Landes Baden-Württemberg; Italy – Istituto Nazionale di

Fisica Nucleare (INFN); Istituto Nazionale di Astrofisica (INAF); Ministero dell'Università e della Ricerca (MUR); CETEMPS Center of Excellence; Ministero degli Affari Esteri (MAE), ICSC Centro Nazionale di Ricerca in High Performance Computing, Big Data and Quantum Computing, funded by European Union NextGenerationEU, reference code CN_00000013; México – Consejo Nacional de Ciencia y Tecnología (CONACYT) No. 167733; Universidad Nacional Autónoma de México (UNAM); PAPIIT DGAPA-UNAM; The Netherlands – Ministry of Education, Culture and Science; Netherlands Organisation for Scientific Research (NWO); Dutch national e-infrastructure with the support of SURF Cooperative; Poland – Ministry of Education and Science, grants No. DIR/WK/2018/11 and 2022/WK/12; National Science Centre, grants No. 2016/22/M/ST9/00198, 2016/23/B/ST9/01635, 2020/39/B/ST9/01398, and 2022/45/B/ST9/02163; Portugal – Portuguese national funds and FEDER funds within Programa Operacional Factores de Competitividade through Fundação para a Ciência e a Tecnologia (COMPETE); Romania – Ministry of Research, Innovation and Digitization, CNCS-UEFISCDI, contract no. 30N/2023 under Romanian National Core Program LAPLAS VII, grant no. PN 23 21 01 02 and project number PN-III-P1-1.1-TE-2021-0924/TE57/2022, within PNCDI III; Slovenia – Slovenian Research Agency, grants P1-0031, P1-0385, I0-0033, N1-0111; Spain – Ministerio de Ciencia e Innovación/Agencia Estatal de Investigación (PID2019-105544GB-I00, PID2022-140510NB-I00 and RYC2019-027017-I), Xunta de Galicia (CIGUS Network of Research Centers, Consolidación 2021 GRC GI-2033, ED431C-2021/22 and ED431F-2022/15), Junta de Andalucía (SOMM17/6104/UGR and P18-FR-4314), and the European Union (Marie Sklodowska-Curie 101065027 and ERDF); USA – Department of Energy, Contracts No. DE-AC02-07CH11359, No. DE-FR02-04ER41300, No. DE-FG02-99ER41107 and No. DE-SC0011689; National Science Foundation, Grant No. 0450696, and NSF-2013199; The Grainger Foundation; Marie Curie-IRSES/EPLANET; European Particle Physics Latin American Network; and UNESCO.